Biochimica et Biophysica Acta 1848 (2015) 1127–1138

Contents lists available at ScienceDirect

Biochimica et Biophysica Acta

journal homepage: www.elsevier.com/locate/bbamem

Stimuli responsive polymorphism of C_{12}NO/DOPE/DNA complexes: Effect of pH, temperature and composition

Lukáš Hubčík [a,*], Sergio S. Funari [b], Petra Pullmannová [a,1], Ferdinand Devínsky [c], Daniela Uhríková [a]

[a] Department of Physical Chemistry of Drugs, Faculty of Pharmacy, Comenius University, Odbojárov 10, 832 32 Bratislava, Slovakia
[b] HASYLAB at DESY, Notkestr. 85, D-22607 Hamburg, Germany
[c] Department of Chemical Theory of Drugs, Faculty of Pharmacy, Comenius University, Odbojárov 10, 83232 Bratislava, Slovakia

ARTICLE INFO

Article history:
Received 24 May 2014
Received in revised form 9 January 2015
Accepted 29 January 2015
Available online 7 February 2015

Keywords:
N,N-dimethyldodecylamine-*N*-oxide
Cationic liposome
Small angle X-ray diffraction
DNA
pH responsive polymorphism

ABSTRACT

N,N-dimethyldodecylamine-*N*-oxide (C_{12}NO) is a surfactant that may exist either in a neutral or cationic protonated form depending on the pH of aqueous solutions. Using small angle X-ray diffraction (SAXD) we observe the rich structural polymorphism of pH responsive complexes prepared due to DNA interaction with C_{12}NO/dioleoylphosphatidylethanolamine (DOPE) vesicles and discuss it in view of utilizing the surfactant for the gene delivery vector of a pH sensitive system. In neutral solutions, the DNA uptake is low, and a lamellar L_α phase formed by C_{12}NO/DOPE is prevailing in the complexes at $0.2 \leq C_{12}NO/DOPE < 0.6$ mol/mol. A maximum of ~30% of the total DNA volume in the sample is bound in a condensed lamellar phase L_α^C at C_{12}NO/DOPE = 1 mol/mol and pH 7.2. In acidic conditions, a condensed inverted hexagonal phase H_{II}^C was observed at C_{12}NO/DOPE = 0.2 mol/mol. Commensurate lattice parameters, $a_{HC} \approx d_{LC}$, were detected at $0.3 \leq C_{12}NO/DOPE \leq 0.4$ mol/mol and pH = 4.9–6.4 suggesting that L_α^C and H_{II}^C phases were epitaxially related. While at the same composition but pH ~ 7, the mixture forms a cubic phase (*Pn3m*) when the complexes were heated to 80 °C and cooled down to 20 °C. Finally, a large portion of the surfactant ($C_{12}NO/DOPE > 0.5$) stabilizes the L_α^C phase in C_{12}NO/DOPE/DNA complexes and the distance between DNA strands (d_{DNA}) is modulated by the pH value. Both the composition and pH affect the DNA binding in the complexes reaching up to ~95% of the DNA total amount at acidic conditions.

1. Introduction

Complexes of DNA with cationic liposomes (CL) are intensively studied as potential non-viral vectors for gene therapy [1–4]. Cationic lipids and surfactants strongly interact with the polyanion of DNA due to electrostatic attraction and, also, due to the stabilization of DNA surfactant complexes through hydrophobic interactions between lipophilic moieties of surfactant molecules. The compensation of the negative charge of DNA by cationic species, allows the complex to approach the cytoplasmic membrane. In addition, cationic surfactants have been reported to collapse individual DNA molecules and to form small particles, which allow an efficient internalization of these complexes into the cells [5,6]. The transport mechanism of DNA into the cells includes several key steps. The complex internalized inside the cell by endocytosis has to escape from the endosome through the activated fusion with the endosomal membrane. After the escape from the endosome, DNA must be released by the dissociation of these complexes into the cytoplasm. Whereas for a successful escape from the endosome a high positive surface charge density of complexes is needed as it facilitates the fusion with the negatively charged endosomal membrane, for the dissociation of complexes into the cytoplasm a high surface charge density is undesirable as it increases their stability and prevents complex dissociation [7,8]. One of the ways to overcome this problem is the use of pH-sensitive surfactants with pK_a within the range of 4.5 to 8. These pH-sensitive surfactants are at acidic pH inside the endosomes in their cationic form, which enables the membrane fusion of the complexes with the endosome. At neutral pH, in the cytoplasm, they are mainly in their non-ionic form enabling an easy dissociation of the complex [9–11].

Relationships between the structure of gene delivery vectors and their transfection efficiency have been studied widely for many years, and the conclusions are not all consistent [12–14]. A condensed lamellar phase (L_α^C) with DNA strands packed regularly between cationic phospholipid bilayers [15] and an inverted hexagonal phase where DNA is arranged inside of tubules formed by inverted micelles and packed in hexagonal symmetry (H_{II}^C) [16] are the most discussed structures,

Abbreviations: SAXD, small angle X-ray diffraction; C_{12}NO, *N,N*-dimethyldodecylamine-*N*-oxide; DOPE, dioleoylphosphatidylethanolamine; HT-DNA, DNA from herring testes; L_α^C, condensed lamellar phase; H_{II}^C, condensed hexagonal phase; CL, cationic liposome

* Corresponding author.
E-mail address: hubcik@fpharm.uniba.sk (L. Hubčík).
[1] Present address: Department of Inorganic and Organic Chemistry, Faculty of Pharmacy, Charles University, Heyrovského 1203, 500 05 Hradec Králové, Czech Republic.

http://dx.doi.org/10.1016/j.bbamem.2015.01.020
0005-2736/

although bicontinuous cubic phases [17,18] were also revealed in morphologies of gene delivery vectors. For the L_{α}^{C} phase, the optimal surface charge density of a cationic membrane ($\sigma_M \sim e/100$ Å^2) was found as a key parameter for the fusion of cationic liposome–DNA complexes with the endosomal membrane [7]. X-ray structural studies show that the rate of DNA release from lipoplexes as well as transfection activity correlate well with non-lamellar phase progressions observed in cationic–neutral lipid mixtures [12,14,19]. The transfection behavior of the inverted hexagonal H_{II}^{C} phase of cationic liposome–DNA complexes is independent of the membrane charge density.

N,*N*-dimethyldodecylamine-*N*-oxide ($C_{12}NO$) (Fig. 1) is a non-ionic surfactant in solutions with neutral pH. However a strong polar N – O bond with a high electron density on oxygen yields in the protonation of molecules ($C_{12}N^{+}OH$) at acidic pH (pK ~ 5) [20–23].

$C_{12}NO$ as an amphiphile incorporates into biological membranes and can induce changes of fluidity [24,25] and thickness [26–29] of lipid bilayers. At high concentration, $C_{12}NO$ destabilizes lipid bilayers, and forms non-bilayer phases and mixed micelles [30,31]. Generally, C_nNO (in CnNO, *n* is the number of carbons in the alkyl substituent) displays antimicrobial [25,32], immunomodulatory [33] or antiphotosynthetic activity [34]. Also functions of membrane proteins such as sarcoplasmic reticulum Ca^{2+}-ATPase are modulated [35]. However, all available information on amine oxides demonstrates their low-to-moderate level of toxicity [36–38].

The toxicity of *N*,*N*-dimethylalkylamine oxides expressed as their lowest, still effective concentration at which the growth of the microorganisms is inhibited, or the so called minimum inhibitory concentration (MIC) supports the statement above. For example, the MIC of $C_{12}NO$, the most effective of the C_nNOs, n = 6–18 homologous series, detected at *Escherichia coli* and *Staphylococcus aureus* was found 3–340 times higher [32,39] in comparison to gemini surfactant pentane-1,5-diyl-bis(dodecyldimethylammonium bromide) used in the liposomal DNA delivery vector in transfection experiments [40,41]. In absolute unit scale, Warisnoicharoen et al. [38] found 0.08 mg/ml (~350 μM) as the $C_{12}NO$ concentration that caused 50% cell death (i.e. IC_{50}) tested on human bronchial epithelium cells. Recently, 0.023 mg/ml of $C_{12}NO$ (100 μM) was recognized as the concentration causing the increase in mammalian cells' lethality [37].

Among the C_nNO homological series, $C_{12}NO$ is widely used in pharmaceutical and cosmetic formulations, as detergent in household dishwashing liquids and surface cleaners and in various areas of industry [36,37,42]. Due to its large use, the concentration of C_nNO in some rivers in Japan was monitored, and was found at 0.01–0.07 μg/l (<0.3 nM if related to $C_{12}NO$ only) as declared in the report of the Japan Soap and Detergent Association (JSDA, Tokyo, Japan), cited in Fukunaga et al. ([37] and references therein). For comparison, common concentrations of cationic surfactants in transfection experiments are in the range of 2–50 μM [43,44].

DNA interaction with $C_{12}NO$ or $C_{12}NO$/phospholipid is poorly reported in literature. The first experiments, focused on DNA coil–globule phase transition in the presence of $C_{12}NO$ and modulated by pH, came from the group of Lindman [45]. Using fluorescence microscopy for visualizing the DNA compaction process by surfactant micelles, they observed that the minimum surfactant concentration necessary to compact DNA increases with pH. The phase map of DNA/$C_{12}NO$ compaction shows a strong DNA interaction with protonated $C_{12}N^{+}OH$ at pH < 6.4, while DNA coil did not collapse due to the surfactant interaction when pH increases above 7.4. Using SAXS, the authors identified the hexagonal structure in DNA/$C_{12}NO$ complexes at acidic conditions. The experiments thus revealed the strong influence of pH on DNA/$C_{12}NO$ interaction. Turbidimetric and light scattering experiments of Wang et al. [46] analyzed DNA interaction with $C_{12}NO$ micelles focusing on the degree of $C_{12}NO$ protonation and micelle shape as a function of pH. Additional experimental methods, dielectric spectroscopy and circular dichroism [47], fluorescence with pH sensitive probe [48], dynamic light scattering and viscosity measurements [49] were employed with the aim of shedding light into the interaction and establishing the pH range of $C_{12}NO$ micelle protonation sufficient for an effective DNA/$C_{12}NO$ complexation. DNA interaction with the surfactant/lipid mixed system was discussed only by Mel'nikova and Lindman [45]. DNA compaction by unilamellar vesicles prepared from an equimolar $C_{12}NO$/DOPE mixture was followed by fluorescence microscopy. The authors found the mixture more efficient in DNA compaction as compared to the surfactant alone in the same pH range. SAXD experiments have shown a lamellar structure with the repeat distance of 6.28 nm for the DNA/$C_{12}NO$/DOPE complex at $C_{12}NO$/DOPE = 1 mol/mol and pH = 5.5. Under alkaline conditions, pH = 8.5, DNA interaction with vesicles resulted in their aggregation and flocculation as the authors derived from images of the cryo-TEM technique.

Despite the large use of C_nNO in different fields of industry and its non-zero concentration in the environment, very little is known about interactions between the surfactant and biologically important molecules. For many years our workplace studies the biological activity and physico-chemical properties of C_nNO on real systems or models of biological membranes [24,26,28–30,32–35]. Our preliminary static light experiments on the $C_{14}NO$/DNA system confirmed the high pH sensitivity of the surfactant/DNA interaction in good agreement with results described above. SAXD on DNA/$C_{14}NO$/dimyristoylphosphatidylcholine (DMPC) complexes revealed that the distance between DNA strands (d_{DNA}) packed in a condensed lamellar phase can be modulated in the range 6.0–3.8 nm changing pH from 8 to 4, respectively [50].

The present study extends the investigation of the polymorphic behavior of C_nNO/lipid/DNA complexes. We focused our experiments on DNA condensation with $C_{12}NO$/DOPE mixtures as a function of composition, pH and temperature. SAXD experiments revealed a large variety of liquid-crystalline mesophases, differences in their stability as well as in their capability to accommodate DNA when the pH of the solutions changes from neutral to acidic. The binding efficiency of the $C_{12}NO$/DOPE mixture for DNA was examined by UV–vis spectrophotometry. We routed our experiments towards the possibility of utilizing the surfactant for the gene delivery vector of a pH sensitive system. However, we believe that the obtained knowledge about the surfactant–lipid–DNA polymorphism modulated through pH can attract a larger audience from the areas of pharmacy, chemistry or biophysics.

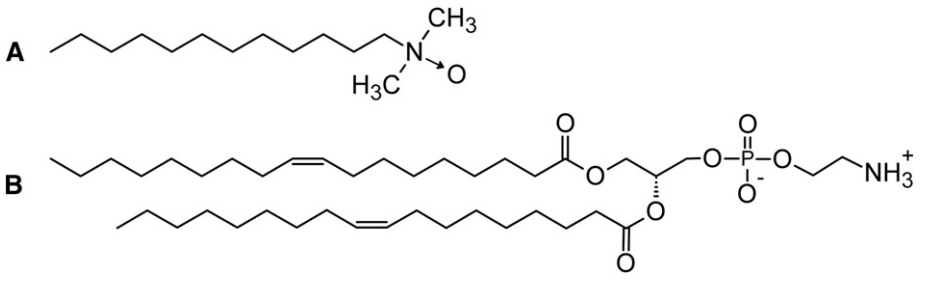

Fig. 1. The structure of *N*,*N*-dimethyldodecylamine-*N*-oxide ($C_{12}NO$) (A) and dioleoylphosphatidylethanolamine (DOPE) (B).

2. Experimental

2.1. Materials

Neutral phospholipid DOPE (1,2-dioleoyl-sn-glycero-3-phosphoethanolamine) was purchased from Avanti Polar Lipids, Inc., USA, and highly polymerized DNA (sodium salt) type XIV from herring testes (HT-DNA, average M_r of nucleotide = 308) was purchased from Sigma-Aldrich, USA. *N,N*-dimethyldodecylamine-*N*-oxide ($C_{12}NO$) was synthesized from *N,N*-dimethyldodecylamine by oxidation with hydrogen peroxide and purified as described by Devínsky et al. [51]. The NaCl of analytical purity and 35% solution of HCl were obtained from Lachema, Brno, Czech Republic. The chemicals were of the analytical grade and were used without further purifications. The aqueous solutions were prepared with redistilled water.

2.2. Preparation of DNA solutions

The solution of DNA was prepared by dissolving HT-DNA in a 150 mM NaCl solution. The precise value of DNA concentration was determined spectrophotometrically (Hewlett Packard 8452A Diode array spectrophotometer), according to the equation $c_{DNA} = A_{260} \cdot 47 \times 10^{-6}$ [g/ml], where A_{260} is the absorbance at wavelength $\lambda = 260$ nm. The concentration of DNA is referred to the molar concentration of DNA bases. The purity of DNA was checked by measuring the absorbance A_λ at $\lambda = 260$ and 280 nm. We obtained the value of $A_{260}/A_{280} = 1.79$.

2.3. Preparation of cationic liposomes

DOPE and $C_{12}NO$ were dissolved in chloroform and mixed to obtain a mixture with the desired molar ratio of $C_{12}NO$/DOPE. Lipid mixtures were dried under a stream of gaseous nitrogen and the residue of chloroform was removed under vacuum. The dry mixtures were hydrated by the solution of HT-DNA in 150 mM NaCl at a molar ratio of $C_{12}NO$/DNA = 1 (mol/base) and the volume of samples was adjusted by 150 mM NaCl to 2 ml. Afterwards samples were homogenized (by vortexing and freezing–thawing). The pH of samples was adjusted by stepwise addition of 50 mM HCl solution. A fully hydrated DOPE was used as a control sample. The samples were stored for 1 week at 6 °C before measurements. The pH of the samples was checked again before the measurements.

2.4. Small angle X-ray diffraction (SAXD) experiments

SAXD experiments were performed at the soft condensed matter beamline A2 at HASYLAB at the Deutsches Elektronen Synchrotron (DESY) in Hamburg (Germany), using a monochromatic radiation with a wavelength of $\lambda = 0.15$ nm. The samples of the $C_{12}NO$/DOPE/DNA complexes were shortly centrifuged. The sedimented precipitate with a few drops of bulk solution was enclosed between two Kapton (Dupont, France) windows of a sample holder for X-ray diffraction. The scattering pattern was recorded using a 2D Mar CCD detector after the minimal 3 min tempering of the samples at selected temperatures. The raw data were calibrated using rat tail collagen [52] and normalized against the incident beam intensity using the purposed-written software A2TOOL. Each diffraction peak of the SAXD region was fitted with a Lorentzian above a linear background using the Peakfit software. Lattice parameters were determined with uncertainty ±0.1 Å or less.

2.5. The capacity of $C_{12}NO$/DOPE/DNA complexes for DNA binding

The fraction of DNA bound by $C_{12}NO$/DOPE liposomes was determined from the supernatant of the samples prepared for SAXD measurements as the difference between the total DNA amount added to the sample and the DNA fraction not bound after the complex formation (the free DNA in the supernatant). UV–vis spectrophotometry was employed for quantitative analysis. Due to the light scattering on uncomplexed vesicles or small aggregates that might occur in the supernatant in spite of the complex separation by short centrifugation, UV–vis spectra were deconvoluted. The procedure is described in [53], and briefly: the light scattering was approximated with a function $A_\lambda = a \cdot \lambda^b$, where a and b are scattering constants. The function is a simplification of Rayleigh scattering. Numerical values of coefficients a and b were obtained using a non-linear least square approximation of absorption spectra out of the absorption band ($\lambda = 320$–500 nm). Then the function was extrapolated to $\lambda < 320$ nm. The DNA absorption maximum (A_{260}) corrected for the light scattering contribution was obtained by a numerical subtraction of extrapolated scattering function from the measured spectrum (for a graphical sketch, see Fig. S1 in Supplementary data).

3. Results and discussion

3.1. The structure of $C_{12}NO$/DOPE/DNA complexes at neutral pH — effect of the composition

At the molecular level, the intercalation of $C_{12}NO$ between DOPE molecules induces changes in two regions: the polar fragment of $C_{12}NO$ (charged at acidic conditions) interacts with polar groups of DOPE yielding a lateral expansion of the interface, while a mismatch between the length of $C_{12}NO$ alkyl substituent and the length of hydrocarbon acyl chains of DOPE (18 carbons) creates defects in the hydrophobic membrane core. These defects are eliminated by chain bending or through trans-gauche isomerization, leading to a decrease of the thickness of the hydrophobic region [28,54]. Generally, the addition of amphiphiles to lipid mixtures affects also the membrane bending rigidity [12], while the increase of the surface charge inhibits the formation of inverted non-lamellar phases [55]. It is worth reminding, that in addition to the elastic properties of the $C_{12}NO$/DOPE membrane, electrostatic interactions between membrane and DNA also play an important role in the aggregation process. As a result, the preferred complexation geometry is generally dictated by a nontrivial interplay between electrostatic and elastic contributions to the free energy of the complexes [56].

Fully hydrated DOPE (Fig. 1) at 20 °C forms an inverted hexagonal phase showing diffraction peaks at reciprocal distances $s_{hk} = 2(h^2 + k^2 - hk)^{1/2} / (a \cdot \sqrt{3})$ (Å^{-1}), where h and k are Miller indices, and $a = 2 / (s_{10} \cdot \sqrt{3})$ (Å) is a lattice parameter determined from the position of H_{II} (1,0) peak's maximum (Fig. 2). The lattice parameter of DOPE at 20 °C is $a_H = 75.9$ Å. The structure of $C_{12}NO$/DOPE/DNA complexes was investigated in the range of molar ratios of $0.1 \le C_{12}NO/DOPE \le 1$ in solutions under neutral, pH ~ 7.2, and slightly acidic pH ≈ 5–6 conditions. The samples at pH ~ 7.2 were prepared without any pH adjustment.

Representative diffractograms of $C_{12}NO$/DOPE/DNA complexes are shown in Fig. 2A. At neutral pH the fraction of protonated $C_{12}N^+OH$ is low [20–23] (Fig. S2 in Supplementary data) and thus DNA binding is weak [45,46,50]. With the aim of emphasizing changes induced by DNA complexation, panel B in Fig. 2 displays diffractograms of $C_{12}NO$/DOPE mixtures prepared at the same conditions (without DNA). At a molar ratio of $C_{12}NO$/DOPE = 0.1 we observe peaks belonging to an inverted hexagonal phase (H_{II}) and a lamellar phase (L_1) (Fig. 2A, B). From their positions, structural parameters were determined and are summarized in Table S1 (Supplementary data). The lattice parameter a_H ~ 78 Å of the H_{II} phase in both structures (Fig. 2A, B) is due to the presence of a surfactant. It is slightly larger compared to that of the hexagonal phase of DOPE ($a_H = 75.9$ Å). The repeat distance d of the L_1 phase determined as $d = 1/s_1$, where s_1 is the first order peak's maximum of the L_1 phase ($L_1(1)$), is the same in both structures, d ~ 53 Å. An increase of $C_{12}NO$ content to $C_{12}NO$/DOPE = 0.2 mol/mol induces a significant decrease of the volume fraction of the H_{II} phase, and the L_1 phase

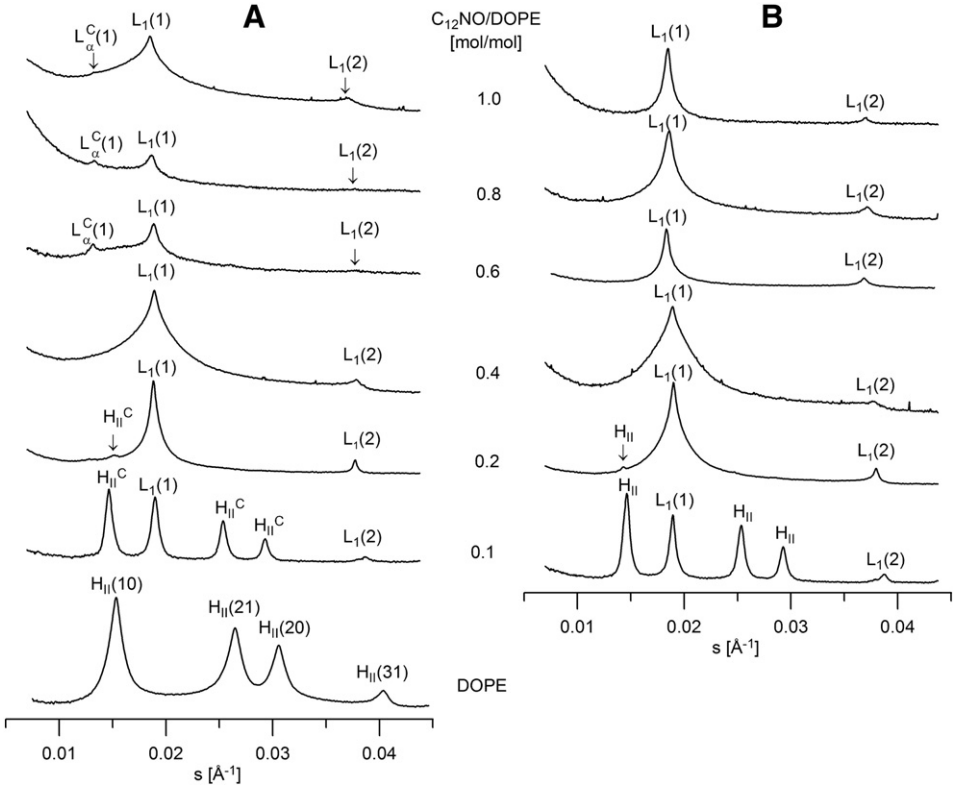

Fig. 2. Diffractograms of DOPE and A) $C_{12}NO$/DOPE/DNA complexes and B) $C_{12}NO$/DOPE mixtures; hydrated by 150 mM NaCl at pH ~ 7.2 and 20 °C. Intensities are in logarithmic scale.

becomes dominant. However, the obtained parameters show differences between the two H_{II} structures (Fig. 2A, B): in $C_{12}NO$/DOPE/DNA complexes the lattice parameter $a_{HC} = 76.2$ Å indicates a more tightly packed structure in comparison to the system at $C_{12}NO$/DOPE = 0.1 mol/mol, while we found an increase of a_H to 81.0 Å for the $C_{12}NO$/DOPE–water mixture. We attribute these small differences in a to changes of the radius of water cylinders arranged in a hexagonal symmetry. The radius of water cylinders of the H_{II} phase of DOPE at 20 °C is 21.6 Å [57]. Thus hydrated DNA strands with a diameter of ~25 Å [15] can be easily accommodated in water cylinders of the H_{II} phase. DNA–cationic liposome systems show a significant reduction of the radius of water cylinders in the H_{II}^C phase (down to 13–14 Å), due to DNA condensation [16,56]. DOPE–DNA interaction without any cationic mediator is rather weak, and lattice parameters of the H_{II} phase display an insignificant difference (Δa); we found $\Delta a = a_{DOPE} - a_{DOPE\ +\ DNA} \sim 1.1\ (\pm 0.1)$ Å. The obtained structural parameters indicate DNA complexation into the H_{II} phase at a molar ratio of $C_{12}NO$/DOPE = 0.2, however the interaction is weak, the DNA trapped content is low (see below), and changes in structural parameters are insignificant. In both systems, the H_{II} phase vanished with a further increase in the molar ratio of $C_{12}NO$/DOPE to 0.3 (not shown). The increasing content of $C_{12}NO$ in mixtures affects also the packing of the L_1 phase: the peaks of the L_1 phase became wider most likely due to less positional order of the elementary cell arrangement, a consequence of lamellae fluctuations. In both systems, the repeat distance of the L_1 phase remained unchanged up to molar ratios of $C_{12}NO$/DOPE ≤ 0.5, then d increases gradually up to $d \sim 54$ Å at $C_{12}NO$/DOPE = 1 mol/mol (for details see Table S1, Supplementary data). At molar ratios of $C_{12}NO$/DOPE ≥ 0.5 the structures clearly differ. The diffractograms of $C_{12}NO$/DOPE/DNA complexes (Fig. 2A) show the presence of another lamellar phase that we identified as a condensed lamellar phase L_α^C with DNA strands packed between the lipid bilayers. Its repeat distance d_{LC} slightly decreases (from 76.3 to 74.9 Å) with an increasing fraction of $C_{12}NO$ in the complexes. The significantly higher repeat distance of the L_α^C phase compared to d of the L_1 phase (system without DNA) confirms the correct phase assignment and $\Delta d = d_{LC} - d > 20$ Å indicates enough room for DNA strand intake. Diffractograms of $C_{12}NO$/DOPE/DNA ≥ 0.6 mol/mol complexes (Fig. 2A) show only one tiny peak (at s ~ 0.013 $Å^{-1}$) identified as the first order peak of the L_α^C phase; its low intensity indicates that the volume fraction of this phase is small. Intensities of diffractograms in Fig. 2 are plotted in logarithmic scale. However, irrespective of the scale, the diffraction peaks related to the complexes structure are broad and their intensities are lower in comparison to those in diffractograms of the $C_{12}NO$/DOPE mixtures (Fig. 2B). The quality of diffractograms thus also gives evidence that the DNA binding between $C_{12}NO$/DOPE lamellae is weak, and each bilayer fluctuates considerably around its mean position, keeping the long range order preserved.

The interaction between DNA and the lipid bilayer is mediated by the fraction of $C_{12}NO$ molecules in their protonated form ($C_{12}N^+OH$). The dissociation constant of $C_{12}NO$ monomers is pK ~ 5, however the dissociation property of the amine oxide group can be shifted because of its environment. The value of $pK_m \sim 5.9$ was reported for $C_{12}NO$ molecules bound in micelles [22]. Mel'nikova and Lindman [45] assumed that also the DNA itself supports the surfactant ionization due to cooperative electrostatic interactions. They observed the onset of the complexation at pH ~ 7.4 in both studied systems, when DNA interacted with $C_{12}NO$ micelles, or mixed vesicles $C_{12}NO$/DOPE (1:1 mol/mol). The authors reported that at pH ≤ 6.4 all of the DNA content was bound into the complexes. Similar "shifts" in the degree of ionization were observed at DNA–weak polybase interactions [58] and predicted theoretically by Monte Carlo simulations [59]. It was found that the drug apparent pK changes in the presence of lipid membranes [60,61]. In our system, molecules of $C_{12}NO$ are intercalated between molecules of DOPE. Zeta potential measurements indicate 0 mV at pH ~ 7.5 for vesicles prepared at $C_{12}NO$/DOPE = 0.4 mol/mol in an aqueous solution at low ionic strength (see Fig. S2 in Supplementary data).

Generally, the formation of cationic liposome–DNA (CL–DNA) complexes is driven by the strong electrostatic attraction between the cationic lipid headgroups and negatively charged phosphate groups of the DNA backbone. This attraction is mediated by the release of the

small mobile ("counter") ions into solution upon DNA–lipid complexation, and the concomitant gain in their entropy. This gain is maximal at the "isoelectric point" when the total lipid charge exactly balances the total DNA charge [62]. Indeed, experiments confirmed that CL–DNA complexes at isoelectric composition show excellent stability allowing the tuning of DNA–DNA distance in a one-phase complex through cationic/helper lipid ratio. Out of isoelectric composition the system easily separates either into complex + excess of liposomes or complex + excess of DNA [63]. High ionic strength reduces the fraction of bound DNA in the complexes, and the isoelectric point is attained at a DNA/cationic surfactant ratio which is lower than the one that can be estimated by calculation based on nominal charges of CLs and DNA [64]. In our experiments, C_{12}NO/DOPE/DNA complexes were prepared at a constant ratio of DNA/C_{12}NO = 1:1 (mol/base), i.e. nominal isoelectric composition supposing total protonation of C_{12}NO, in order to avoid "a large" excess of DNA at high pH and its possible osmotic effect (in synergy with the high ionic strength of our aqueous media). Thus the total mass of DNA in each sample increased with the C_{12}NO/DOPE molar ratio, and the mass of DOPE was kept constant.

Fig. 3A shows the mass of bound DNA in milligrams per milligram of C_{12}NO/DOPE mixture. Despite a poor degree of C_{12}NO protonation at pH ~ 7.2, its effect on DNA intake into the complexes is evident. The mass of bound DNA per mg of lipid increases stepwisely with the molar ratio of C_{12}NO/DOPE reaching up to ~0.1 mg DNA/mg lipid at the molar ratio of C_{12}NO/DOPE = 0.6. Above this level, DNA binding remains almost unchanged taking into account the uncertainty of the measurement. The insert (Fig. 3B) displays the same dependence when the bound DNA is expressed as a percentage of the total DNA in the sample, and as such gives a view of the efficiency of DNA condensation. Surprisingly, the dependence show an extremity, indicating the highest efficiency in DNA binding (~90%) when complexes are formed at a composition of C_{12}NO/DOPE = 0.2 mol/mol. SAXD (Fig. 2A) displays marked structural changes at this molar ratio. The portion of C_{12}NO molecules intercalated between the lipid molecules was sufficient to transform the structure of the complex from hexagonal to lamellar packing. It seems that the lamellar phase even with a low C_{12}NO content, binds DNA more effectively than does the hexagonal phase. Comparing dependencies on both plots, we can conclude that the further increase of the surfactant portion in the mixture supports DNA binding (up to 0.1 mg/mg lipid mixture), but in regard to its total content the binding efficiency decreases. This decrease of DNA binding efficiency suggests that, at low ionization of C_{12}NO binding depends on the portion of the lipid as well.

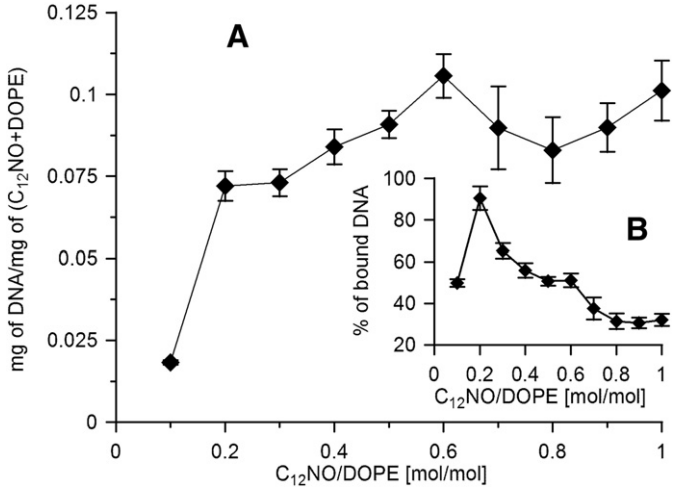

Fig. 3. A) Dependence of DNA in C_{12}NO/DOPE/DNA complexes at pH ~ 7.2 expressed as mg of bound DNA per mg of C_{12}NO/DOPE lipid mixture; B) C_{12}NO/DOPE binding efficiency, % of bound DNA related to the total DNA mass in the sample. Data are presented as average ± S.D.

Note, that at pH ~ 7.2, SAXD identifies a small volume fraction of the L_α^C phase with DNA condensed between the lipid lamellae only at C_{12}NO/DOPE ≥ 0.6 mol/mol. Surprisingly, the amount of bound DNA is relatively high in all samples with a predominant lamellar structure, which indicates that in addition to electrostatic interaction other binding mechanisms can also take place, namely cooperative binding due to DNA strand adsorption on the surface of the structures formed in the mixture [49]. Mel'nikova and Lindman [45] visualized the process of aggregation through fluorescence microscopy and reported a substantial fraction of DNA molecules adsorbed on the surface of the vesicles or entrapped between vesicles. Thus DNA binding to C_{12}NO/DOPE at neutral pH, particularly at low C_{12}NO fraction is closer to a model of "bead on string" [15] picturing the DNA stored decorated with attached liposomes, which was proposed originally by Felgner [65,66]. In our system the "beads" are mainly composed of multilamellar C_{12}NO/DOPE vesicles with a low fraction of DNA that may be condensed between a few upper bilayers.

3.2. Thermal stability of C_{12}NO/DOPE/DNA complexes at neutral pH

Fully hydrated DOPE at 20 °C forms an inverted hexagonal phase (Fig. 2A) not modified by temperature increase, despite a decrease of the unit cell size, a_H. The lamellar packing of DOPE was observed when cooling the lipid below 20 °C, although literature values reported for the $H_{II} \leftrightarrow L_\alpha$ phase transition temperature (T_{LH}) range from −4 to 16 °C [67]. The presence of additives can shift T_{LH} to higher values. Indeed, even a small amount of our surfactant (C_{12}NO/DOPE = 0.1 and 0.2 mol/mol) shifts the $L_\alpha \rightarrow H_{II}$ phase transition of DOPE, and at 20 °C we see both phases (Fig. 2). A further increase in C_{12}NO concentration stabilizes the lamellar structure in the complexes.

We followed structural changes in C_{12}NO/DOPE/DNA complexes during heating and cooling in the temperature range 20–80–20 °C. Complexes prepared at molar ratios of C_{12}NO/DOPE = 0.2–0.6 and pH ~ 7.2 showed clearly phase transitions during heating (to 80 °C) and cooling back to 20 °C. As an example, in Fig. 4 we present diffractograms of C_{12}NO/DOPE/DNA complexes at C_{12}NO/DOPE = 0.4 mol/mol. During heating, a phase transition from the lamellar L_1 (nomenclature according to Fig. 2 and related text) to the H_{II} phase was observed at ~60 °C (Fig. 4). All our complexes at composition C_{12}NO/DOPE ≤ 0.6 mol/mol showed a $L_\alpha \rightarrow H_{II}$ phase transition when heated up to 80 °C, and T_{LH} increased with increasing C_{12}NO content.

Moreover, at ~70–80 °C in addition to the hexagonal phase, diffractograms show new peaks at small s ($s < 0.013$ Å^{-1}) for complexes prepared at molar ratios of C_{12}NO/DOPE = 0.2–0.6. The new structure, a cubic phase, progressed in the cooling process (down to 20 °C). Peaks assigned to positions $\sqrt{2}$, $\sqrt{3}$, $\sqrt{4}$, $\sqrt{6}$, $\sqrt{8}$, $\sqrt{9}$, $\sqrt{10}$, $\sqrt{12}$, $\sqrt{14}$ and $\sqrt{16}$ fit extremely well a bicontinuous cubic phase of the *Pn3m* space group. The best organization and stability of the *Pn3m* phase is observed in samples at molar ratios of C_{12}NO/DOPE = 0.3 and 0.4 where it is the only remaining structure after cooling to 20 °C. In samples prepared at other molar ratios of C_{12}NO/DOPE, the cubic phase is present in coexistence with phases that were observed in samples during the initial heating. This newly formed *Pn3m* phase showed very good stability in time. Even after 3–4 days there were no signs of any phase transition back to the lamellar or hexagonal phase and also no changes in its lattice parameter. The lattice parameter of the *Pn3m* phase (a_P) was determined from the slope of the plot of the peak positions vs. $\sqrt{\left(h^2+k^2+l^2\right)}$, passing by the origin (0,0) (see Supplementary data, Fig. S3). The smallest lattice parameter (a_P ~ 153 Å) of the *Pn3m* phase is found in complexes at molar ratios of C_{12}NO/DOPE = 0.3 and 0.4 (where the *Pn3m* phase is the only observed phase) while for complexes with composition at the edges of this region (C_{12}NO/DOPE = 0.2 and 0.6 mol/mol), the lattice parameter is substantially larger, $a_P \geq 180$ Å. According to literature the formation of the *Pn3m* phase is

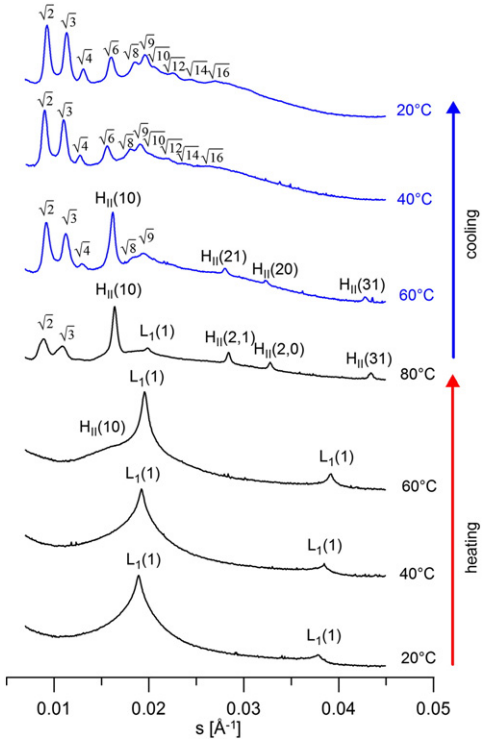

Fig. 4. Diffractograms of C_{12}NO/DOPE/DNA complexes formed at a molar ratio of C_{12}NO/DOPE = 0.4 at pH = 7.2 in 150 mM NaCl at selected temperatures during the heating to 80 °C (black lines) and cooling back to 20 °C (blue lines). Intensities are in logarithmic scale.

observed in pure hydrated DOPE and other phosphatidylethanolamines after several tens or hundreds of heating and cooling cycles around the temperature of $L_\alpha \rightarrow H_{II}$ phase transition [68,69]. The phase transition into cubic phase energetically lies between the lamellar phase and the hexagonal phase [68]. However the difficulty involved in settling DOPE into the cubic phase suggests that the corresponding free energy valley is isolated by relatively large kinetic barriers [68]. In contrast to the pure DOPE, our DNA complexes at C_{12}NO/DOPE = 0.2–0.6 mol/mol form the cubic phase already during the first heating–cooling cycle. At these molar ratios the content of C_{12}NO would lower the kinetic barriers between the free energy valleys of cubic and hexagonal phases.

We did not observe peaks related to cubic phases in diffractograms of C_{12}NO/DOPE/DNA complexes for C_{12}NO/DOPE > 0.6 mol/mol. The only observed changes after the heating–cooling process were in the intensities and shape of the peaks. The peaks depict a larger amplitude and are narrower suggesting a better positional order of the elementary cells.

Bicontinuous cubic phases (like *Pn3m*) are formed by a pair of interpenetrating but noncontacting aqueous channels separated by a single, continuous lipid bilayer. Tuning of the aqueous nanochannel sizes constitutes a way for controlling their encapsulation capacity of biomolecules [70,71]. Our experiment confirmed such capability for C_{12}NO, when the C_{12}NO/DOPE molar ratio dependent lattice parameter varies in the range a_P ~ 153–180 Å and provides enough room for DNA accommodation. Accommodation of proteins (hemoglobin, immunoglobulin, ferritin) [72] and siRNA [18] reported recently, suggests two ways of packing: either the encapsulation of small proteins occurs in aqueous channels without perturbation of the cubosome structure, or the entrapment of proteins with sizes larger than the water channel diameters occurs via a "nanopocket defects" mechanism and spontaneous nanocubosome generation in the interior of the cubic lipid/protein assembly.

Parallel to the SAXD experiment we investigated the amount of DNA incorporated in our system and its changes during the heating–cooling cycle. The C_{12}NO/DOPE/DNA complex at a composition of C_{12}NO/DOPE = 0.4 mol/mol and pH ~ 7.2 was selected for the experiment and the portion of bound DNA was determined by UV–vis spectra. The analysis indicated DNA uptake during heating: almost three times more DNA is trapped in complex at 60 °C. However, a further increase of temperature, up to 80 °C, the temperature at which SAXD shows transformation into non-lamellar structures, resulted in DNA release. We determined ~15% less DNA bound in regards to its initial amount. DNA was also released from the complex along with the cooling, and ~30% less in comparison to the initial bound DNA content was detected when the complex was cooled back to 20 °C. We did not observe any temperature induced denaturation of DNA during the experiment.

Cubic phases exist in equilibrium with excess water; they are viscous, and these properties are likely responsible for their ability to protect incorporated drugs and proteins from degradation. Transfection experiments using the delivery vector forming a cubic phase are not frequent in literature and results differ. Koynova et al. [73] reported a much lower transfection efficiency when genetic material was loaded into the cubic structure formed by cationic lipid 1,2-dierucoyl-*sn*-glycero-3-ethylphosphocholine in comparison to the system with lamellar packing. Contrary to these results, Leal et al. [18] found a very good transfection efficiency of cationic lipids forming cubic phases of *Ia3d* symmetry with a lattice parameter a_P ~ 150 Å for siRNA delivery. More experiments are necessary to unravel the transfection efficiency of cubic phases and their utilization for genetic material delivery.

3.3. The structure of C_{12}NO/DOPE/DNA complexes at acidic pH — effect of the composition

In acidic solutions, the C_{12}NO molecules are protonated, and the surfactant behaves as a cationic agent. Increasing surfactant molar fraction, increases the surface charge of C_{12}NO/DOPE mixture, and both the C_{12}NO content and its charge inhibit formation of inverted non-lamellar phases. On the other hand, both DNA and the mixture have a tendency to compensate their charges at the interaction, and thus complexation geometry results from the interplay between electrostatics and elasticity of the constituent lipid layer.

The diffractograms of the C_{12}NO/DOPE/DNA complexes prepared in solutions at acidic conditions, pH = 5–6 are shown in Fig. 5. As previously, the content of C_{12}NO increased in the range of molar ratios of $0.1 \leq C_{12}NO/DOPE \leq 1$. We show again the diffractogram of DOPE alone (at the bottom). DNA complexation with the lipid mixture in solutions at acidic pH resulted in different structures when compared to neutral conditions, Fig. 2.

At a molar ratio of C_{12}NO/DOPE = 0.1, C_{12}NO/DOPE/DNA complexes form two inverted hexagonal phases, with lattice parameters a_H = 77.3 Å and a_{HC} = 73.3 Å. The first close to the lattice parameter of pure DOPE (a_H = 75.9), is a phase without DNA inserted in the tubules formed by the mixture. The surfactant content is low at this molar ratio, but repulsion between $C_{12}N^+OH$ molecules result in a small increase of the radii of water cylinders. The second hexagonal phase has as smaller lattice parameter, a_{HC} = 73.3 Å. The effective DNA screening of charges at condensation in H_{II} tubules results in the reduction of the elementary cell dimension, as discussed in Section 3.1. The phase is thus identified as a condensed inverted hexagonal phase (H_{II}^C). Likely, in our system, the electrostatic attraction between DNA and the $C_{12}N^+OH$/DOPE layer leads to a reduction of the water content inside of the H_{II}^C tubules. At C_{12}NO/DOPE = 0.2 mol/mol the only phase observed is H_{II}^C as the content of $C_{12}N^+OH$ is sufficient to stabilize this phase in the whole volume of the mixture. A further increase in the molar ratio to C_{12}NO/DOPE = 0.3, induced again structural changes, and in addition to the H_{II}^C phase we detected a condensed lamellar phase (L_α^C). Note that, its repeat distance, d_{LC} = 71.8 Å, is smaller than that observed for L_α^C phases d_{LC} (76.3–74.9 Å) in complexes with much higher C_{12}NO content (C_{12}NO/DOPE = 0.5–1 mol/mol), prepared at pH ~ 7.2. Fig. 5 shows that a further increase in the molar ratio of C_{12}NO/DOPE supports the L_α^C phase

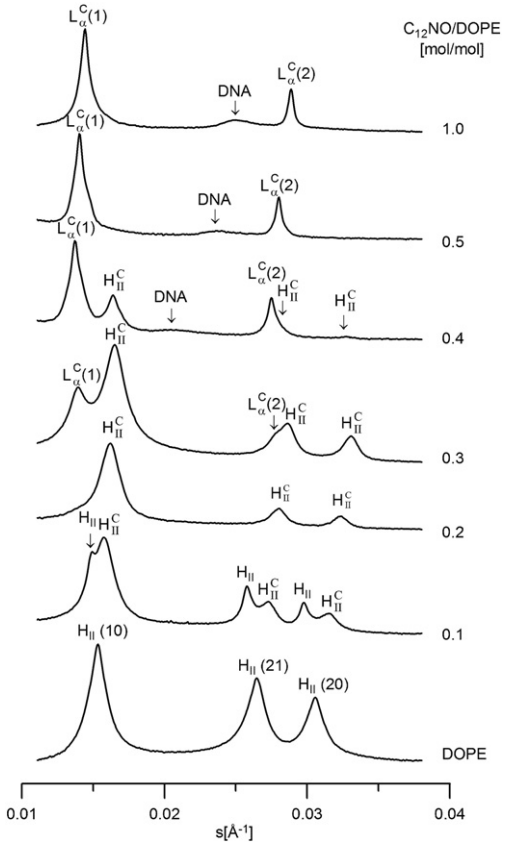

Fig. 5. Diffractograms of DOPE and C_{12}NO/DOPE/DNA complexes at pH = 5–6 prepared in 150 mM NaCl and measured at 20 °C. Intensities are in logarithmic scale.

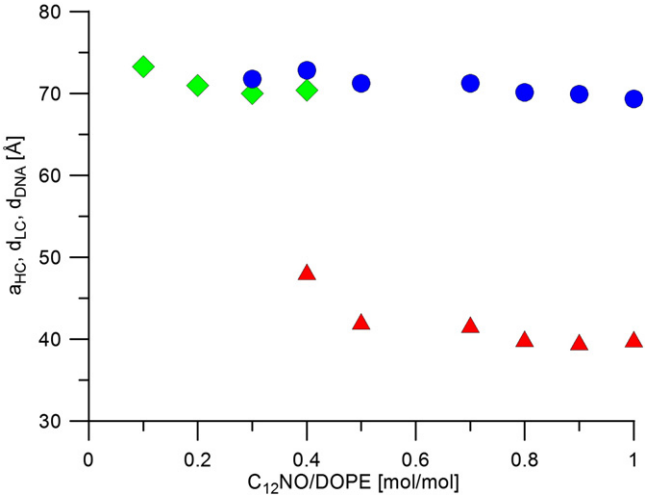

Fig. 6. Structural parameters of C_{12}NO/DOPE/DNA complexes prepared in solutions at pH 5–6 vs. C_{12}NO/DOPE molar ratio: The lattice parameter a_{HC} of the H_{II}^C phase (♦), the repeat distance d_{LC} of the L_α^C phase (●) and the DNA–DNA distance d_{DNA} (▲) (measured at 20 °C).

propagation and concomitant reduction of the volume fraction of H_{II}^C. Finally, at a molar ratio of C_{12}NO/DOPE ≥ 0.5 we observe only the L_α^C phase. In addition, diffractograms of the complexes with the predominant L_α^C phase, show a small broad peak, related to the regularly packed DNA strands between lipid bilayers. The distance between DNA strands (d_{DNA}) is expressed as $d_{DNA} = 1/s_{DNA}$, where s_{DNA} is the position of the DNA peak's maximum.

Comparing Figs. 2 and 5, one can see that the $H_{II} \rightarrow L_\alpha$ transition driven by the C_{12}NO content is shifted to higher molar ratios of C_{12}NO/DOPE in acidic solutions. This finding could be used for designing complexes that need the lamellar packing at neutral pH and transform into the H_{II}^C phase when pH drops to acidic. For example, the $L_\alpha \rightarrow H_{II}$ transition at acidic pH can provide a more efficient endosomal escape of DNA, as the formation of the H_{II}^C phase can accelerate a fusion of the complexes with the endosomal membrane [74].

The structural parameters of individual phases observed in the C_{12}NO/DOPE/DNA complexes (at 20 °C) prepared at pH = 5–6 are shown in Fig. 6. We see, that both lattice parameters, a of the H_{II}^C phase as well as d_{LC} of the L_α^C phase slightly decrease with an increasing C_{12}NO fraction in complexes. Two effects support the observed decrease: the increasing C_{12}NO content with shorter alkyl chains in comparison to DOPE reduces the bilayer thickness (as discussed in Section 3.1) and the tighter DNA packing between opposite charged bilayers. The DNA–DNA distance, d_{DNA}, also decreases with increasing content of charged surfactant molecules, i.e. DNA strands follow the surface charge density of C_{12}NO/DOPE membranes, as predicted in the theoretical work of May and Ben-Shaul [62]. To summarize, at acidic conditions, our C_{12}NO/DOPE/DNA complexes show a behavior typical of complexes prepared with cationic surfactants or cationic lipids [15,16,75]. Moreover, their polymorphic behavior (H_{II}^C or L_α^C phase) can be modulated by changes in the C_{12}NO/DOPE ratio.

3.4. Effect of pH on the structure of C_{12}NO/DOPE/DNA complexes

C_{12}NO/DOPE/DNA complexes are very sensitive to changes of pH in solutions. Important structural differences manifested in Figs. 2 and 5 motivated us to inspect closer the pH impact on the C_{12}NO/DOPE/DNA structure. Two molar ratios were selected for these experiments, C_{12}NO/DOPE = 0.4 and 1, and the pH of solutions was changed in the range ~4.5–7. Typical diffractograms taken at 20 °C are shown in Fig. 7A, B. Already at first sight, diffractograms show a richer structural polymorphism for complexes at C_{12}NO/DOPE = 0.4 mol/mol (Fig. 7A). Let us inspect pH induced changes with increasing acidity, i.e. increasing C_{12}NO protonation: we see that the L_1 phase identified as a lamellar phase without accommodated DNA strands (thoroughly discussed in Section 3.1), or its fraction, was detected by X-ray only at pH > 6.8. Already a small drop of pH from neutral 7.3 to 6.9 increased the protonation degree of C_{12}NO and a condensed lamellar phase, L_α^C, is clearly recognized, and is the only phase detected at pH = 6.8. The diffractogram of the complex prepared at pH = 6.4, signalizes the onset of a new structure. Heating the sample to higher temperatures (Fig S4 in Supplementary data) helped us to identify the structure as an inverted condensed hexagonal H_{II}^C phase. Diffractograms of complexes prepared in the pH range 6.4–5 show that both, L_α^C and H_{II}^C, are present in the C_{12}NO/DOPE/DNA complexes and their volume fractions varied with pH. Volume fractions of both phases expressed through normalized integral intensities of the first peaks indicate the maximum in the H_{II}^C content at pH ~ 5.3. We did not detect the H_{II}^C phase in the diffractogram of the complexes prepared at pH = 4.6. The structural parameters obtained from deconvoluted diffraction patterns are plotted in Fig. 8 (empty symbols). Note that the coexistence of L_α^C and H_{II}^C phases is detected in the range of pH = 4.9–6.4. The obtained repeat distance, d_{LC}, of the L_α^C phase is commensurate with the lattice parameter, a_{HC}, of the H_{II}^C phase ($d_{LC} \approx a_{HC}$). Their values $|d_{LC} - a|$, differ by 0.2–1.6 Å, with the highest deviation (~1.6 Å) at pH = 6.4. The closeness of the structural parameters indicates a "connection" of both phases through the common scattering plane. This facilitates the transition because the lipid within a certain scattering plane does not have to rearrange, but continues to exist within the new structure. Actually, diffractograms show a systematic overlap of the $L_\alpha^C(2)$ peak with $H_{II}^C(21)$. The schematic drawing for such an epitaxial relationship, observed in our system is shown in Fig. 9. Lamellar to hexagonal phase transition in a pure lipid system or their mixtures has been systematically studied [76–79]. Mainly due to differences in hydration, commensurate lattices in pure lipid systems are exceptional (if any). Molecules of cationic additives

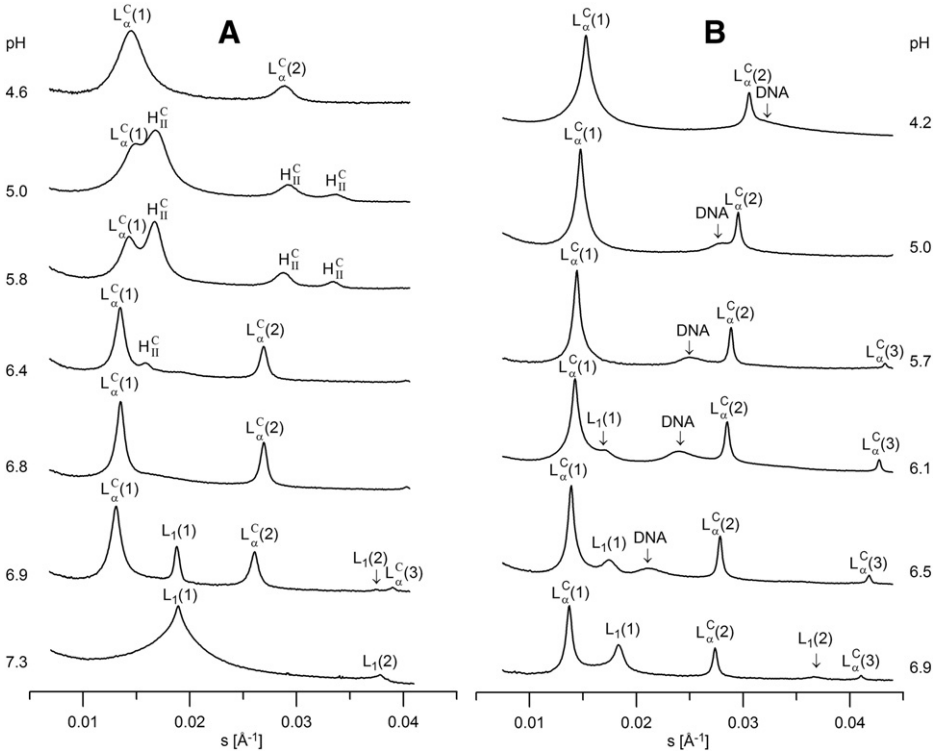

Fig. 7. Diffractograms of C_{12}NO/DOPE/DNA complexes hydrated by 150 mM NaCl at various pHs and 20 °C, at composition: A) C_{12}NO/DOPE = 0.4 mol/mol and B) C_{12}NO/DOPE = 1 mol/mol. Intensities are in logarithmic scale.

inserted between molecules of helper lipid (DOPE) and tight DNA binding to the charged lipid layers modulate structural parameters of both, lamellar as well as hexagonal phases, in such a way that, at specific compositions of the mixture, their parameters might be commensurate. Koltover et al. [16] noted epitaxially matched $d_{LC} \approx a_{HC}$ at a specific composition of a DOPE/cationic lipid mixture. In our system, Fig. 6 indicates commensurate lattice parameters at the composition of $0.3 \leq C_{12}$NO/DOPE ≤ 0.4 mol/mol, and moreover we found that the transfer of the lipid mixture between the two phases can be modulated by subtle pH changes within the range ΔpH ~ 1.5. This also supports the view of a low energetic barrier between both structures and a strong tendency of our C_{12}NO/DOPE mixtures (at specific molar ratios) to adopt non-lamellar phases with highly curved surfaces. Note that the lattice parameter a_{HC} of the H_{II}^C phase drops from ~76 Å (the pure lipid) to ~70 Å, and indicates the effective DNA condensation due to the charge compensation. In addition to the electrostatic character of the binding and lower hydration of the DOPE polar head group, its readiness to form intermolecular hydrogen bonds and the "conical" geometrical shape of the molecule itself promote a tendency to form structures with high curvature [76]. Heating the complex C_{12}NO/DOPE/DNA at C_{12}NO/DOPE = 0.4 mol/mol in solution at slightly acidic conditions (pH ~ 6), all of the mixture transforms to the H_{II}^C phase (Fig. S4, Supplementary data). We observe a further reduction of a_{HC} (~67 Å at 80 °C) because of the water expelled out of the cylinders of the H_{II}^C phase at heating (Fig. S5, Supplementary data). Note that the complex at the same composition and pH ~ 7.2 resulted in a cubic phase (Fig. 4) when heated up to 80 °C.

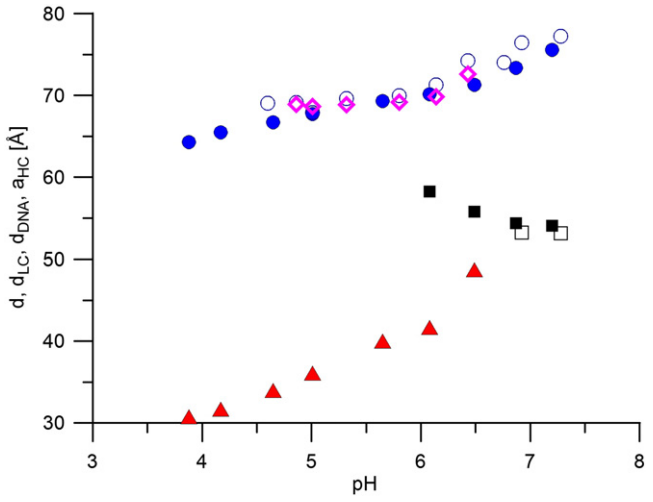

Fig. 8. Structural parameters of C_{12}NO/DOPE/DNA complexes as a function of pH. The complexes were prepared at C_{12}NO/DOPE = 0.4 mol/mol (empty symbols) and C_{12}NO/DOPE = 1 mol/mol (full symbols): repeat distance of the L_1 phase d (■); repeat distance of the L_α^C phase d_{LC} (●); DNA–DNA distance in the L_α^C phase d_{DNA} (▲); lattice parameter of the H_{II}^C phase a_{HC} (♦) (20 °C).

Fig. 7B shows diffractograms of C_{12}NO/DOPE/DNA complexes at C_{12}NO/DOPE = 1 mol/mol in the pH range 4.2–6.9. Concerning polymorphism, the documented behavior is more trivial. The condensed lamellar phase, L_α^C, is the predominant structure in the complexes in the whole pH range. The volume fraction of the L_1 phase (lamellar phase without DNA) gradually decreases with the increasing acidity of the solutions. The L_1 phase is detected up to pH = 6.1 which is a smaller value compared to complexes prepared at C_{12}NO/DOPE = 0.4 mol/mol. Indeed, the higher content of C_{12}NO needs more H^+ charges for its protonation which reflects in lower pH. Simultaneously, the fraction of $C_{12}N^+OH$ is sufficiently high already at pH = 6.5, to keep DNA strands regularly ordered between lamellae of the L_α^C phase, as manifested by the peak related to DNA–DNA packing. The DNA peak is gradually shifted to higher s values, thus DNA–DNA distance (d_{DNA}) decreases with an increasing surface charge modulated through pH. Structural parameters are represented in Fig. 8. We can see that, in the whole pH range studied, there is an overlap in the values of the repeat distances d_{LC} (empty and full circles) of the L_α^C phase obtained for C_{12}NO/DOPE/DNA complexes prepared at both molar ratios of C_{12}NO/DOPE = 0.4

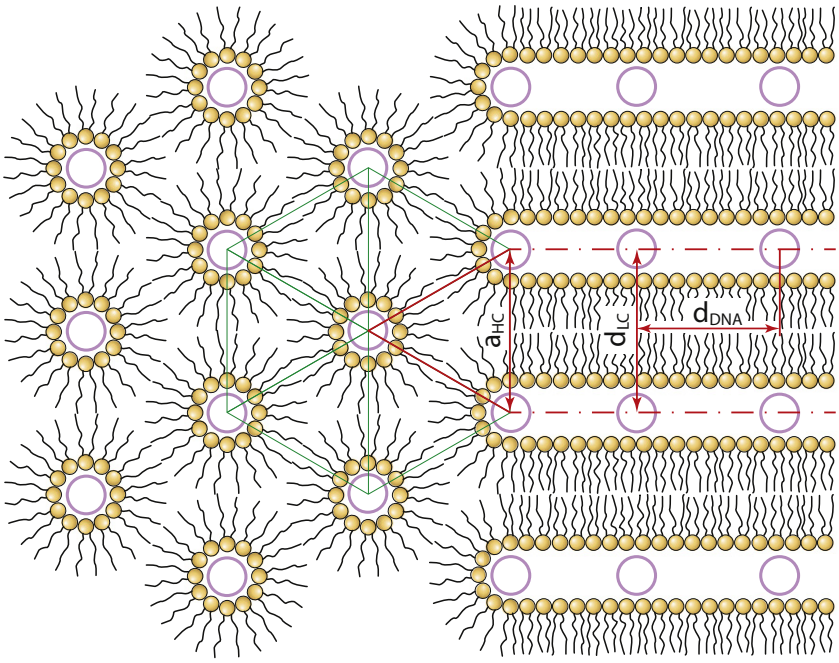

Fig. 9. Schematic drawing of epitaxial relationship between L_α^C and H_{II}^C phases in C_{12}NO/DOPE/DNA complexes at C_{12}NO/DOPE = 0.4 mol/mol and pH range 4.9–6.4.

and 1. It indicates that the massive increase in the surfactant content in the mixture (from 0.4 to 1 mol/mol) stabilizes the L_α^C phase, however the repeat distances do not change significantly. d_{DNA} decreases from ~50 to 30 Å accompanied by a pH drop from 6.5 to 4. The obtained values of both parameters, repeat distance d_{LC} and d_{DNA}, correlate well with those typically observed for DNA/cationic liposome complexes [15,16,80].

Fig. 10 displays the capability of the C_{12}NO/DOPE mixture for DNA binding as a function of pH. The DNA binding was determined for complexes prepared at C_{12}NO/DOPE = 0.4 and 1 mol/mol. The fraction of DNA bound in the complexes was determined using spectrophotometry (Section 2.5), and is expressed as a percentage of total DNA mass added to the mixture. At both compositions, the C_{12}NO/DOPE mixture shows strong DNA binding in solutions at acidic conditions: more than 90% of the total DNA amount is condensed in the complexes when pH < 6.8. The obtained dependences correlate well with the surface charge of

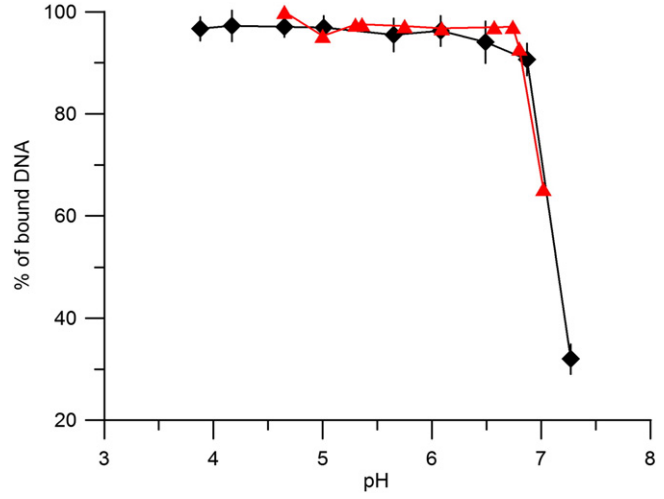

Fig. 10. The DNA binding in C_{12}NO/DOPE/DNA complexes at the composition: C_{12}NO/DOPE = 0.4 (▲) and C_{12}NO/DOPE = 1 mol/mol (♦) as a function of pH (20 °C). The amount of bound DNA is expressed as a percentage of total DNA mass added to the mixture.

C_{12}NO/DOPE vesicles derived from zeta potential measurements performed at the mixture composition C_{12}NO/DOPE = 0.4 mol/mol in aqueous solution at low ionic strength (5 mM NaCl). At pH range 5–7, zeta potential slightly decreases with increasing pH, showing 22 ± 8 mV at pH 7. At pH > 7, zeta potential values dropped down, oscillating at 0 ± 8 mV when pH ~ 7.5. Indeed, the binding efficiency decreases sharply in solutions at neutral pH; we found only ~30% of DNA bound in the complexes at C_{12}NO/DOPE = 1 mol/mol at pH = 7.3. Fig. 10 shows that the DNA binding efficiencies were similar at both compositions of the C_{12}NO/DOPE mixture.

Our experiments revealed that the "loading capacity" of the C_{12}NO/DOPE mixture for DNA depends on both the molar fraction of the surfactant in the mixture and pH. In an absolute scale, the trapped DNA varies between 0.02 mg DNA/1 mg mixture in C_{12}NO/DOPE = 0.1 mol/mol, pH ~ 7.2 and 0.31 mg DNA/1 mg in C_{12}NO/DOPE = 1 mol/mol at acidic solutions with pH < 6.5. DNA uptake into the C_{12}NO/DOPE mixture shows strong pH dependence in the pH range ~ 6.5–7.5 which indicates its potential utilization as a pH responsive delivery system.

The extracellular and intracellular pH profile of biological systems is greatly affected by diseases. The pH at systematic sites of infections, primary tumors and metastasized tumors is lower than the pH of normal tissues. For example, pH drops from 7.4 under normal conditions to 6.5 60 h after the onset of an inflammatory reaction [81]. Also cellular components such as the cytoplasm, endosomes, lysosomes, endoplasmic reticulum, etc. are known to maintain their own characteristic pH values. The pathway of the gene–vector complex is accompanied by a drop in pH from physiological (pH ~ 7.4) to the acidic in lysosomes (pH ~ 4.5). Let us shortly inspect this pathway in view of the obtained knowledge about the C_{12}NO/DOPE mixture: the pH in endosomes varies from 6.0 to 6.5 in early endosomes to pH = 4.5–5.5 in late endosomes and lysosomes [82]. At this pH, more than 90% of the DNA is bound in complexes with C_{12}NO/DOPE. The incorporation of DNA inside the lipid mixture (L_α^C or H_{II}^C phase) protects it against degradation by endosomal enzymes. Moreover, for successful escape from the endosome, a high positive surface charge density of the complexes is required in order to facilitate fusion with the negatively charged endosomal membrane. At such pH, the C_{12}NO/DOPE/DNA complex with a sufficient C_{12}NO content forms L_α^C, or we found the coexistence of both L_α^C and H_{II}^C phases (at C_{12}NO/DOPE = 0.4 mol/mol). The release

of the complex to the cytoplasm is accompanied by a pH change to 7.0–7.4. At neutral pH only a small fraction of $C_{12}NO$ molecules is protonated and our experiments confirm a dramatic reduction in the DNA amount trapped in the complexes. However, additional experiments are necessary to test the possible utilization of $C_{12}NO$ in transfection.

4. Conclusions

In solutions at neutral pH, *N*,*N*-dimethyldodecylamine-*N*-oxide ($C_{12}NO$) is a non-ionic surfactant; however at acidic conditions the molecule becomes cationic due to its protonation. Our experiments were aimed to investigate the structural polymorphism of complexes formed due to DNA interaction with the $C_{12}NO$/DOPE mixture. The composition of $C_{12}NO$/DOPE was modulated through the molar ratio of the two constituents in the range $0.1 \leq C_{12}NO/DOPE \leq 1$ mol/mol. SAXD revealed rich structural polymorphism of $C_{12}NO$/DOPE/DNA complexes when the pH of solutions is changed from neutral (~7.3) to acidic (~4.8). In summary: with an increasing $C_{12}NO$ content, the hydrated $C_{12}NO$/DOPE mixture shows $H_{II} \rightarrow L_\alpha$ phase transition in solutions at neutral pH. The coexistence of L_α and a condensed lamellar phase L_α^C with DNA incorporated in the structure was detected in the complexes. A low degree of the $C_{12}NO$ protonation at neutral pH results in poor DNA binding; 0.1 mg of DNA/1 mg of the lipid mixture was found as the maximal DNA uptake at $C_{12}NO/DOPE = 1$ mol/mol. However heating the complexes with a composition of $0.2 \leq C_{12}NO/DOPE \leq 0.6$ mol/mol induced massive structural changes and a cubic phase of the *Pn3m* space group was detected. At acidic conditions $C_{12}NO$/DOPE/DNA complexes show a similar behavior as those prepared with cationic surfactants or cationic lipids. The high content of protonated $C_{12}NO$ in the complexes stabilizes the lamellar structure and the DNA–DNA distance was modulated through changes in pH. The condensed inverted hexagonal phase H_{II}^C is found in complexes with a low $C_{12}NO$ content ($C_{12}NO/DOPE = 0.2$ mol/mol) at acidic conditions. A noteworthy coexistence of L_α^C and H_{II}^C phases commensurate with the lattice parameters, $a_{HC} \approx d_{LC}$, indicating an epitaxial relationship between both phases, is found in complexes at the mixture composition of $0.3 \leq C_{12}NO/DOPE \leq 0.4$ mol/mol and pH = 4.9–6.4. The ratio between populations of the two phases changes with pH. H_{II}^C prevails during heating. The capability of complexes for DNA binding at acidic conditions reaches ~95% of the total amount of DNA in the sample.

It is postulated that effective pH responsive formulations should be able to change a property in a narrow pH window. Two pH windows were detected in our system: the DNA uptake changes significantly due to a pH drop from 7.3 to 6.5 at each composition of the mixture for $C_{12}NO/DOPE \geq 0.2$ mol/mol; and the $L_\alpha^C \rightarrow H_{II}^C$ phase transition at a specific composition of the complexes modulated through subtle pH changes in the range 6.4–4.9.

Strong pH dependent polymorphic behavior and a large variety of liquid-crystalline phases, and the capability of the surfactant–lipid mixtures to uptake (and release) anionic molecules revealed in our study suggest the utilization of C_nNO/lipid mixtures for designing genetic material delivery vectors as discussed in this paper, but also for nanocarriers for targeted drug delivery or cosmetics. A number of studies, especially in cancer therapy, have shown that stimuli responsive nanocarriers reveal significant advantages.

Transparency document

The Transparency document associated with this article can be found in the online version.

Acknowledgement

This work is dedicated to Professor P. Balgavý. The authors are grateful for the many years of scientific support and guidance. The authors also thank Assoc. Prof. M. Pisárčik for his assistance with zeta potential measurements. The research leading to these results has received funding from the European Community's Seventh Framework Programme (FP7/2007-2013) under grant agreement no. 226716 (HASYLAB project II-20100372 EC), by the JINR project 04-4-1069-2009/2014 and grants APVV 0212-10, APVV 0516-12, VEGA 1/1224/12 and 1/0159/11 and FaF UK/27/2014.

Appendix A. Supplementary data

Supplementary data to this article can be found online at http://dx.doi.org/10.1016/j.bbamem.2015.01.020.

References

[1] P.L. Felgner, T.R. Gadek, M. Holm, R. Roman, H.W. Chan, M. Wenz, et al., Lipofection: a highly efficient, lipid-mediated DNA-transfection procedure, Proc. Natl. Acad. Sci. U. S. A. 84 (1987) 7413–7417.
[2] L. Wasungu, D. Hoekstra, Cationic lipids, lipoplexes and intracellular delivery of genes, J. Control. Release 116 (2006) 255–264. http://dx.doi.org/10.1016/j.jconrel.2006.06.024.
[3] S. Zhang, Y. Xu, B. Wang, W. Qiao, D. Liu, Z. Li, Cationic compounds used in lipoplexes and polyplexes for gene delivery, J. Control. Release 100 (2004) 165–180. http://dx.doi.org/10.1016/j.jconrel.2004.08.019.
[4] G. Caracciolo, H. Amenitsch, Cationic liposome/DNA complexes: from structure to interactions with cellular membranes, Eur. Biophys. J. 41 (2012) 815–829. http://dx.doi.org/10.1007/s00249-012-0830-8.
[5] S.M. Meľnikov, V.G. Sergeyev, K. Yoshikawa, Transition of double-stranded DNA chains between random coil and compact globule states induced by cooperative binding of cationic surfactant, J. Am. Chem. Soc. 117 (1995) 9951–9956. http://dx.doi.org/10.1021/ja00145a003.
[6] R. Dias, B. Lindman, DNA Interactions with Polymers and Surfactants, John Wiley & Sons, Inc., Hoboken, New Jersey, 2008.
[7] A.J. Lin, N.L. Slack, A. Ahmad, C.X. George, C.E. Samuel, C.R. Safinya, Three-dimensional imaging of lipid gene-carriers: membrane charge density controls universal transfection behavior in lamellar cationic liposome–DNA complexes, Biophys. J. 84 (2003) 3307–3316. http://dx.doi.org/10.1016/S0006-3495(03)70055-1.
[8] A. Ahmad, H.M. Evans, K. Ewert, C.X. George, C.E. Samuel, C.R. Safinya, New multivalent cationic lipids reveal bell curve for transfection efficiency versus membrane charge density: lipid–DNA complexes for gene delivery, J. Gene Med. 7 (2005) 739–748. http://dx.doi.org/10.1002/jgm.717.
[9] V. Budker, V. Gurevich, J.E. Hagstrom, F. Bortzov, J.A. Wolff, pH-sensitive, cationic liposomes: a new synthetic virus-like vector, Nat. Biotechnol. 14 (1996) 760–764. http://dx.doi.org/10.1038/nbt0696-760.
[10] Y. Sato, H. Hatakeyama, Y. Sakurai, M. Hyodo, H. Akita, H. Harashima, A pH-sensitive cationic lipid facilitates the delivery of liposomal siRNA and gene silencing activity in vitro and in vivo, J. Control. Release 163 (2012) 267–276. http://dx.doi.org/10.1016/j.jconrel.2012.09.009.
[11] I.M. Hafez, S. Ansell, P.R. Cullis, Tunable pH-sensitive liposomes composed of mixtures of cationic and anionic lipids, Biophys. J. 79 (2000) 1438–1446.
[12] C.R. Safinya, K. Ewert, A. Ahmad, H.M. Evans, U. Raviv, D.J. Needleman, et al., Cationic liposome–DNA complexes: from liquid crystal science to gene delivery applications, Phil. Trans. R. Soc. A 364 (2006) 2573–2596. http://dx.doi.org/10.1098/rsta.2006.1841.
[13] B. Ma, S. Zhang, H. Jiang, B. Zhao, H. Lv, Lipoplex morphologies and their influences on transfection efficiency in gene delivery, J. Control. Release 123 (2007) 184–194http://dx.doi.org/10.1016/j.jconrel.2007.08.022.
[14] R. Koynova, B. Tenchov, Cationic phospholipids: structure–transfection activity relationships, Soft Matter 5 (2009) 3187–3200. http://dx.doi.org/10.1039/B902027F.
[15] J.O. Rädler, I. Koltover, T. Salditt, C.R. Safinya, Structure of DNA–cationic liposome complexes: DNA intercalation in multilamellar membranes in distinct interhelical packing regimes, Science 275 (1997) 810–814.
[16] I. Koltover, T. Salditt, J.O. Rädler, C.R. Safinya, An inverted hexagonal phase of cationic liposome–DNA complexes related to DNA release and delivery, Science 281 (1998) 78–81.
[17] R. Koynova, H.S. Rosenzweig, L. Wang, M. Wasielewski, R.C. MacDonald, Novel fluorescent cationic phospholipid, O-4-napthylimido-1-butyl-DOPC, exhibits unusual foam morphology, forms hexagonal and cubic phases in mixtures, and transfects DNA, Chem. Phys. Lipids 129 (2004) 183–194. http://dx.doi.org/10.1016/j.chemphyslip.2004.01.003.
[18] C. Leal, N.F. Bouxsein, K.K. Ewert, C.R. Safinya, Highly efficient gene silencing activity of siRNA embedded in a nanostructured gyroid cubic lipid matrix, J. Am. Chem. Soc. 132 (2010) 16841–16847. http://dx.doi.org/10.1021/ja1059763.
[19] R. Koynova, B. Tenchov, L. Wang, R.C. Macdonald, Hydrophobic moiety of cationic lipids strongly modulates their transfection activity, Mol. Pharm. 6 (2009) 951–958. http://dx.doi.org/10.1021/mp8002573.
[20] K.W. Herrmann, Micellar properties and phase separation in dimethyldodecylamine oxide–sodium halide–water systems, J. Phys. Chem. 68 (1964) 1540–1546. http://dx.doi.org/10.1021/j100788a047.
[21] H. Maeda, M. Tsunoda, S. Ikeda, Electric and nonelectric interactions of a nonionic–cationic micelle, J. Phys. Chem. 78 (1974) 1086–1090. http://dx.doi.org/10.1021/j100604a008.

[22] R. Kakehashi, S. Yamamura, N. Tokai, T. Takeda, K. Kaneda, K. Yoshinaga, et al., Hydrogen ion titration of long alkyl chain amine oxide micelles, J. Colloid Interface Sci. 243 (2001) 233–240. http://dx.doi.org/10.1006/jcis.2001.7884.

[23] A. Búcsi, J. Karlovská, M. Chovan, F. Devínsky, D. Uhríková, Determination of pK a of *N*-alkyl-*N*, *N*-dimethylamine-*N*-oxides using ^{1}H NMR and ^{13}C NMR spectroscopy, Chem. Pap. 68 (2014) 842–846. http://dx.doi.org/10.2478/s11696-013-0517-3.

[24] F. Šeršeň, A. Leitmanová, F. Devínsky, I. Lacko, P. Balgavý, A spin label study of perturbation effects of *N*-(1-methyldodecyl)-*N*, *N*, *N*-trimethylammonium bromide and *N*-(1-methyldodecyl)-*N*, *N*-dimethylamine oxide on model membranes prepared from *Escherichia coli*-isolated lipids, Gen. Physiol. Biophys. 8 (1989) 133–156.

[25] R.E. Glover, R.R. Smith, M.V. Jones, S.K. Jackson, C.C. Rowlands, An EPR investigation of surfactant action on bacterial membranes, FEMS Microbiol. Lett. 177 (1999) 57–62.

[26] M. Dubničková, M. Kiselev, S. Kutuzov, F. Devínsky, V. Gordeliy, P. Balgavý, Effect of *N*-lauryl-*N*, *N*-dimethylamine *N*-oxide on dimyristoyl phosphatidylcholine bilayer thickness: a small-angle neutron scattering study, Gen. Physiol. Biophys. 16 (1997) 175–188.

[27] D.J. Barlow, M.J. Lawrence, T. Zuberi, S. Zuberi, R.K. Heenan, Small-angle neutron-scattering studies on the nature of the incorporation of polar oils into aggregates of *N*, *N*-dimethyldodecylamine-*N*-oxide, Langmuir 16 (2000) 10398–10403. http://dx.doi.org/10.1021/la0002233.

[28] J. Karlovská, K. Lohner, G. Degovics, I. Lacko, F. Devínsky, P. Balgavý, Effects of nonionic surfactants *N*-alkyl-*N*, *N*-dimethylamine-*N*-oxides on the structure of a phospholipid bilayer: small-angle X-ray diffraction study, Chem. Phys. Lipids 129 (2004) 31–41. http://dx.doi.org/10.1016/j.chemphyslip.2003.11.003.

[29] M. Belička, N. Kučerka, D. Uhríková, A.K. Islamov, A.I. Kuklin, F. Devínsky, et al., Effects of *N*, *N*-dimethyl-*N*-alkylamine-*N*-oxides on DOPC bilayers in unilamellar vesicles: small-angle neutron scattering study, Eur. Biophys. J. 43 (2014) 179–189. http://dx.doi.org/10.1007/s00249-014-0954-0.

[30] D. Uhríková, N. Kucerka, A. Islamov, V. Gordeliy, P. Balgavý, Small-angle neutron scattering study of *N*-dodecyl-*N*, *N*-dimethylamine *N*-oxide induced solubilization of dioleoylphosphatidylcholine bilayers in liposomes, Gen. Physiol. Biophys. 20 (2001) 183–189.

[31] U. Kragh-Hansen, M. le Maire, J.V. Møller, The mechanism of detergent solubilization of liposomes and protein-containing membranes, Biophys. J. 75 (1998) 2932–2946. http://dx.doi.org/10.1016/S0006-3495(98)77735-5.

[32] F. Devínsky, A. Kopecka-Leitmanová, F. Sersen, P. Balgavý, Cut-off effect in antimicrobial activity and in membrane perturbation efficiency of the homologous series of *N*, *N*-dimethylalkylamine oxides, J. Pharm. Pharmacol. 42 (1990) 790–794.

[33] M. Bukovský, D. Mlynarčik, V. Ondráčková, Immunomodulatory activity of amphiphilic antimicrobials on mouse macrophages, Int. J. Immunopharmacol. 18 (1996) 423–426. http://dx.doi.org/10.1016/S0192-0561(96)00040-9.

[34] F. Šeršeň, P. Balgavý, F. Devínsky, Electron spin resonance study of chloroplast photosynthetic activity in the presence of amphiphilic amines, Gen. Physiol. Biophys. 9 (1990) 625–633.

[35] J. Karlovská, D. Uhríková, N. Kucerka, J. Teixeira, F. Devínsky, I. Lacko, et al., Influence of *N*-dodecyl-*N*, *N*-dimethylamine *N*-oxide on the activity of sarcoplasmic reticulum Ca(2+)-transporting ATPase reconstituted into diacylphosphatidylcholine vesicles: effects of bilayer physical parameters, Biophys. Chem. 119 (2006) 69–77. http://dx.doi.org/10.1016/j.bpc.2005.09.007.

[36] S.K. Singh, M. Bajpai, V.K. Tyagi, Amine oxides: a review, J. Oleo Sci. 55 (2006) 99–119.

[37] E. Fukunaga, Y. Ohiwa, M. Yamada, A. Sumi, M. Satoh, Y. Oyama, Effects of *N*, *N*-dimethyldodecylamine-*N*-oxide on some cellular parameters of rat thymocytes, Nat. Sci. Res. 28 (2014) 21–24.

[38] W. Warisnoicharoen, A.B. Lansley, M.J. Lawrence, Toxicological evaluation of mixtures of nonionic surfactants, alone and in combination with oil, J. Pharm. Sci. 92 (2003) 859–868. http://dx.doi.org/10.1002/jps.10335.

[39] F. Devínsky, I. Lacko, F. Bitterová, D. Mlynarčík, Quaternary ammonium-salts. 18. Preparation and relationship between structure, IR spectral characteristics, and antimicrobial activity of some new bis-quaternary isosters of 1,5-pentanediammonium dibromides, Chem. Pap. 41 (1987) 803–814.

[40] I. Badea, R. Verrall, M. Baca-Estrada, S. Tikoo, A. Rosenberg, P. Kumar, et al., In vivo cutaneous interferon-γ gene delivery using novel dicationic (Gemini) surfactant–plasmid complexes, J. Gene Med. 7 (2005) 1200–1214. http://dx.doi.org/10.1002/jgm.763.

[41] M. Muñoz-Úbeda, S.K. Misra, A.L. Barrán-Berdón, S. Datta, C. Aicart-Ramos, P. Castro-Hartmann, et al., How does the spacer length of cationic Gemini lipids influence the lipoplex formation with plasmid DNA? Physicochemical and biochemical characterizations and their relevance in gene therapy, Biomacromolecules 13 (2012) 3926–3937. http://dx.doi.org/10.1021/bm301066w.

[42] F. Devínsky, Amine oxides. XVII. Nonaromatic amine oxides: their use in organic syntheses and industry, Acta Fac. Pharm. Univ. Comen. 40 (1985) 63–83.

[43] E. Mornet, N. Carmoy, C. Lainé, L. Lemiègre, T. Le Gall, I. Laurent, et al., Folate-equipped nanolipoplexes mediated efficient gene transfer into human epithelial cells, Int. J. Mol. Sci. 14 (2013) 1477–1501. http://dx.doi.org/10.3390/ijms14011477.

[44] E. Uchida, H. Mizuguchi, A. Ishii-Watabe, T. Hayakawa, Comparison of the efficiency and safety of non-viral vector-mediated gene transfer into a wide range of human cells, Biol. Pharm. Bull. 25 (2002) 891–897. http://dx.doi.org/10.1248/bpb.25.891.

[45] Y.S. Mel'nikova, B. Lindman, pH-controlled DNA condensation in the presence of dodecyldimethylamine oxide, Langmuir 16 (2000) 5871–5878. http://dx.doi.org/10.1021/la991382t.

[46] Y. Wang, P.L. Dubin, H. Zhang, Interaction of DNA with cationic micelles: effects of micelle surface charge density, micelle shape, and ionic strength on complexation and DNA collapse, Langmuir 17 (2001) 1670–1673. http://dx.doi.org/10.1021/la0010673.

[47] A. Bonincontro, S. Marchetti, G. Onori, A. Santucci, Complex formation between DNA and dodecyl-dimethyl-amine-oxide induced by pH, Chem. Phys. Lett. 370 (2003) 387–392. http://dx.doi.org/10.1016/S0009-2614(03)00074-5.

[48] L. Goracci, R. Germani, G. Savelli, D.M. Bassani, Hoechst 33258 as a pH-sensitive probe to study the interaction of amine oxide surfactants with DNA, Chembiochem 6 (2005) 197–203. http://dx.doi.org/10.1002/cbic.200400196.

[49] S. Marchetti, G. Onori, C. Cametti, DNA condensation induced by cationic surfactant: a viscosimetry and dynamic light scattering study, J. Phys. Chem. B 109 (2005) 3676–3680. http://dx.doi.org/10.1021/jp044867l.

[50] D. Uhríková, O. Tlčimuka, A. Lengyel, S.S. Funari, I. Lacko, P. Balgavý, DNA condensation in presence of *N*-tetradecyl-*N*,*N*-dimethylamine-*N*-oxide: pH dependence, Surfactants and Dispersed Systems in Theory and Practice Proceedings, Faculty of Chemistry, Wrocław University of Technology, Książ Castle, 2007, pp. 393–396.

[51] F. Devínsky, I. Lacko, A. Nagy, Ľ. Krasnec, Amine oxides. I. Synthesis, ^{1}H-n.m.r., and infrared spectra of 4-alkylmorpholine-*N*-oxides, Chem. Pap. 32 (1978) 106–115.

[52] N. Roveri, A. Bigi, P.P. Castellani, E. Foresti, M. Marchini, R. Strocchi, Study of rat tail tendon by X-ray diffraction and freeze-etching technics, Boll. Soc. Ital. Biol. Sper. 56 (1980) 953–959.

[53] A. Lengyel, D. Uhríková, M. Klacsová, P. Balgavý, DNA condensation and its thermal stability influenced by phospholipid bilayer and divalent cations, Colloids Surf. B: Biointerfaces 86 (2011) 212–217. http://dx.doi.org/10.1016/j.colsurfb.2011.04.001.

[54] P. Balgavý, F. Devínsky, Cut-off effects in biological activities of surfactants, Adv. Colloid Interface Sci. 66 (1996) 23–63.

[55] R.N. Lewis, R.N. McElhaney, Surface charge markedly attenuates the nonlamellar phase-forming propensities of lipid bilayer membranes: calorimetric and (31) P-nuclear magnetic resonance studies of mixtures of cationic, anionic, and zwitterionic lipids, Biophys. J. 79 (2000) 1455–1464. http://dx.doi.org/10.1016/S0006-3495(00)76397-1.

[56] S. May, D. Harries, A. Ben-Shaul, The phase behavior of cationic lipid–DNA complexes, Biophys. J. 78 (2000) 1681–1697.

[57] M.W. Tate, S.M. Gruner, Temperature dependence of the structural dimensions of the inverted hexagonal (HII) phase of phosphatidylethanolamine-containing membranes, Biochemistry 28 (1989) 4245–4253. http://dx.doi.org/10.1021/bi00436a019.

[58] A.V. Kabanov, V.A. Kabanov, Interpolyelectrolyte and block ionomer complexes for gene delivery: physico-chemical aspects, Adv. Drug Deliv. Rev. 30 (1998) 49–60. http://dx.doi.org/10.1016/S0169-409X(97)00106-3.

[59] F. Carnal, S. Stoll, Adsorption of weak polyelectrolytes on charged nanoparticles. Impact of salt valency, pH, and nanoparticle charge density. Monte Carlo simulations, J. Phys. Chem. B 115 (2011) 12007–12018. http://dx.doi.org/10.1021/jp205616e.

[60] S. Schreier, W.A. Frezzatti, P.S. Araujo, H. Chaimovich, I.M. Cuccovia, Effect of lipid membranes on the apparent pK of the local anesthetic tetracaine. Spin label and titration studies, Biochim. Biophys. Acta 769 (1984) 231–237.

[61] A. Watts, T.W. Poile, Direct determination by ^{2}H-NMR of the ionization state of phospholipids and of a local anaesthetic at the membrane surface, Biochim. Biophys. Acta 861 (1986) 368–372.

[62] S. May, A. Ben-Shaul, Modeling of cationic lipid–DNA complexes, Curr. Med. Chem. 11 (2004) 151–167. http://dx.doi.org/10.2174/0929867043456142.

[63] I. Koltover, T. Salditt, C.R. Safinya, Phase diagram, stability, and overcharging of lamellar cationic lipid–DNA self-assembled complexes, Biophys. J. 77 (1999) 915–924.

[64] K.K. Son, D.H. Patel, D. Tkach, A. Park, Cationic liposome and plasmid DNA complexes formed in serum-free medium under optimum transfection condition are negatively charged, Biochim. Biophys. Acta 1466 (2000) 11–15.

[65] P.L. Felgner, G.M. Ringold, Cationic liposome-mediated transfection, Nature 337 (1989) 387–388. http://dx.doi.org/10.1038/337387a0.

[66] H. Gershon, R. Ghirlando, S.B. Guttman, A. Minsky, Mode of formation and structural features of DNA–cationic liposome complexes used for transfection, Biochemistry 32 (1993) 7143–7151.

[67] R. Koynova, M. Caffrey, Phases and phase transitions of the hydrated phosphatidylethanolamines, Chem. Phys. Lipids 69 (1994) 1–34.

[68] E. Shyamsunder, S.M. Gruner, M.W. Tate, D.C. Turner, P.T.C. So, C.P.S. Tilcock, Observation of inverted cubic phase in hydrated dioleoylphosphatidylethanolamine membranes, Biochemistry 27 (1988) 2332–2336. http://dx.doi.org/10.1021/bi00407a014.

[69] B. Tenchov, R. Koynova, G. Rapp, Accelerated formation of cubic phases in phosphatidylethanolamine dispersions, Biophys. J. 75 (1998) 853–866. http://dx.doi.org/10.1016/S0006-3495(98)77574-5.

[70] B. Angelov, A. Angelova, V.M. Garamus, G. Lebas, S. Lesieur, M. Ollivon, et al., Small-angle neutron and X-ray scattering from amphiphilic stimuli-responsive diamond-type bicontinuous cubic phase, J. Am. Chem. Soc. 129 (2007) 13474–13479. http://dx.doi.org/10.1021/ja072725.

[71] A. Angelova, B. Angelov, R. Mutafchieva, S. Lesieur, P. Couvreur, Self-assembled multicompartment liquid crystalline lipid carriers for protein, peptide, and nucleic acid drug delivery, Acc. Chem. Res. 44 (2010) 147–156. http://dx.doi.org/10.1021/ar100120v.

[72] J.C. Shah, Y. Sadhale, D.M. Chilukuri, Cubic phase gels as drug delivery systems, Adv. Drug Deliv. Rev. 47 (2001) 229–250.

[73] R. Koynova, L. Wang, R.C. Macdonald, Cationic phospholipids forming cubic phases: lipoplex structure and transfection efficiency, Mol. Pharm. 5 (2008) 739–744. http://dx.doi.org/10.1021/mp800011e.

[74] I.M. Hafez, P.R. Cullis, Roles of lipid polymorphism in intracellular delivery, Adv. Drug Deliv. Rev. 47 (2001) 139–148.

[75] P. Pullmannová, S.S. Funari, F. Devínsky, D. Uhríková, The DNA–DNA spacing in Gemini surfactants–DOPE–DNA complexes, Biochim. Biophys. Acta 1818 (2012) 2725–2731. http://dx.doi.org/10.1016/j.bbamem.2012.05.021.

[76] J.M. Seddon, Structure of the inverted hexagonal (HII) phase, and non-lamellar phase transitions of lipids, Biochim. Biophys. Acta 1031 (1990) 1–69.
[77] D.P. Siegel, R.M. Epand, The mechanism of lamellar-to-inverted hexagonal phase transitions in phosphatidylethanolamine: implications for membrane fusion mechanisms, Biophys. J. 73 (1997) 3089–3111. http://dx.doi.org/10.1016/S0006-3495(97)78336-X.
[78] M. Rappolt, A. Hickel, F. Bringezu, K. Lohner, Mechanism of the lamellar/inverse hexagonal phase transition examined by high resolution X-ray diffraction, Biophys. J. 84 (2003) 3111–3122.
[79] A. Yaghmur, B. Sartori, M. Rappolt, Self-assembled nanostructures of fully hydrated monoelaidin–elaidic acid and monoelaidin–oleic acid systems, Langmuir 28 (2012) 10105–10119. http://dx.doi.org/10.1021/la3019716.
[80] P. Pullmannová, M. Bastos, G. Bai, S.S. Funari, I. Lacko, F. Devínsky, et al., The ionic strength effect on the DNA complexation by DOPC — Gemini surfactants liposomes, Biophys. Chem. 160 (2012) 35–45. http://dx.doi.org/10.1016/j.bpc.2011.09.002.
[81] S. Ganta, H. Devalapally, A. Shahiwala, M. Amiji, A review of stimuli-responsive nanocarriers for drug and gene delivery, J. Control. Release 126 (2008) 187–204. http://dx.doi.org/10.1016/j.jconrel.2007.12.017.
[82] A. Sorkin, M. von Zastrow, Signal transduction and endocytosis: close encounters of many kinds, Nat. Rev. Mol. Cell Biol. 3 (2002) 600–614. http://dx.doi.org/10.1038/nrm883.